



Fractional Order PID Controller Design Using Reference Model on Inverted Pendulum System

M. Serhat Can*¹ , Emrah Sürücü¹ 

¹Tokat Gaziosmanpaşa Üniversitesi, Mühendislik ve Mimarlık Fakültesi, Elektrik-Elektronik Mühendisliği Bölümü, 60250, Tokat, TÜRKİYE

Başyuru/Received: 14/06/2023

Kabul / Accepted: 11/07/2023

Çevrimiçi Basım / Published Online: 11/07/2023

Son Versiyon/Final Version: 14/07/2023

Abstract

The proportional Integral Derivative (PID) controller has three basic parameters: Proportional gain (K_p), Integral gain (K_i) and Derivative gain (K_d). In a conventional PID controller, integral and derivative operators are integer order. The researchers proposed a fractional order PID ($PI^{\lambda}D^{\mu}$) controller by using the fractional integral and derivative operators instead of the integer order integral and derivative operators in the traditional PID controller because it improves the control performance. The $PI^{\lambda}D^{\mu}$ controller has an additional fractional integrator degree (λ) and fractional derivative degree (μ). In this study, the focus is on the design of a fractional-order PID controller according to a reference model in the time domain. Bode's ideal transfer function was used as the reference model. It is aimed to obtain $PI^{\lambda}D^{\mu}$ parameters by minimizing the error between the time domain response of Bode's ideal transfer function model and the output of the system to be controlled by using the optimization method. Genetic Algorithm (GA) optimization was used as the optimization method. The study was carried out as a simulation study on an inverted pendulum system with a single-input multiple-output (SIMO) structure.

Key Words

"Fractional order PID controller, model reference design, inverted pendulum, single input multi output system."

1. Introduction

The proportional Integral Derivative (PID) controller is frequently used in many control applications. It can be designed in P, PI, or PID forms according to the application. In PID form, the error signal is multiplied by the proportional gain (K_p), the error is integrated and multiplied by the integral gain (K_i), the derivative of the error is multiplied by the derivative gain (K_d), and the control signal is obtained by summing these three product values. The K_p , K_i , and K_d gains are the basic characteristics of the PID controller and the performance of the PID controller depends on these three coefficients. The degrees of derivative and integral operators in a conventional PID controller are real and integer values. In the fractional degree PID approach, the degrees of the derivative and integral operators are not integers but are expressed as fractional numbers, and thus the traditional PID controller is expressed as $PI^\lambda D^\mu$. In this notation, λ and μ are degrees of integral and derivative operators, respectively. The $PI^\lambda D^\mu$ controller has a total of five parameters with gain parameters K_p , K_i , K_d , and additional λ and μ parameters. The addition of λ and μ parameters increase the closed-loop performance and durability of the traditional PID controller (O'Dwyer, 2006; Shah & Agashe, 2016).

The operations I^λ and D^μ are fractional integral and fractional derivative operators and fall under fractional order mathematics. The main issue in fractional mathematics is the use of fractional and even complex numbers, rather than the use of integers of the degree of derivative in the derivative operator. The foundations of fractional mathematics are based on the work of Leibniz and L'Hospital. The work of Leibniz and L'Hospital is followed by the work of Liouville in 1832, Holmgren in 1864, and Riemann in 1953. His work on the fractional control structure in the position control of heavy objects, carried out by Tustin in 1958, is the first work presented to the literature in the field of control in engineering. Tustin's work is followed by Manabe's work in 1961 and 1963. In these studies, Manabe touched upon issues related to system control involving fractional integrals. $PI^\lambda D^\mu$ was proposed by Podlubny and in Podlubny studies, it achieved more effective results with controllers than with conventional PID controllers (Podlubny, 1999). Following Podlubny's studies, many studies have been conducted on $PI^\lambda D^\mu$ controller design and applications. Some of these are presented in Table 1 below.

Table 1. Tuning studies for the $PI^\lambda D^\mu$ controller

Luo & Chen, (2009)	Gain crossover frequency and phase margin method
Castillo et al., (2010a)	Time domain method
Castillo et al., (2010b)	Frequency properties method
Hamamcı & Köksal, (2010)	Stability region analysis method
Bouafoura & Braiek, (2010)	Algebraic equations method
Yeroglu & Tan, (2011)	Zigler-Nichols rule and ÅströmHägglund method, and Bode envelopes method
El-Khazali, (2013)	Frequency response method
Azarmi et al., (2015)	Fractional set-point weighted structure method
Muresan et al., (2016)	Vector-based method
Keyser et al., (2016)	Auto-tuning method based on modulus, phase and phase slope of the process method
Deniz et al., (2017)	Fourier eeries method
Keyser et al., (2018)	Robust auto-tuning method based on modulus, phase, phase slope, Nyquist plane method
Deniz et al., (2019)	Standart forms method
Ozyetkin et al., (2020)	Weighted geometrical center method
Shankaran et al., (2022)	Stability region method
Muresan et al., (2022)	Ziegler–Nichols method

In control applications, performance indicators based on the integral of the error variable are used to measure the performance of the designed controller. Integral square error (ISE), Integral absolute error (IAE), Integral time squared error (ITSE), Integral time absolute error (ITAE) are well-known performance indicators based on integral of error. During controller design, controller parameters are changes to minimize the preferred performance index. Optimization method for this process is a very convenient method and optimization method is used in many studies (Doğruer et al. 2017a; Doğruer & Tan, 2020). The error value in the performance indexes can be a direct control system error variable. Or, instead, the error value between the output of a system model that can give the desired value of the system output and the controlled system output can be taken. In the model reference control, an ideal model that provides the desired system output is predetermined and the error between the ideal model and the system output is reduced to zero by adjusting the controller parameters. In the optimization method, one of the performance indexes mentioned above is chosen as the fitness function. During the optimization, the fitness function is minimized by changing the controller parameters (Doğruer et al. 2017b). Thus, the most suitable controller parameters to provide the desired system output are obtained.

In this study, a model-based controller design for the control of a single-input and multiple-output (SIMO) system is discussed. Work was carried out on the inverted pendulum system due to its SIMO structure. The position control of the carrier car (cart) in the inverted pendulum system and the angular position of the pendulum are provided by two separate fractional PID controllers. Bode's fractional order ideal transfer function is used both in the controller design of the cart and in the design of the pendulum controller. Thr Genetic

algorithm optimization algorithm was used to find the most suitable controller parameters. For the fitness function, the ITAE values of the difference between the reference models used for the cart and the pendulum and the outputs of these units were formed by summing the α and β weighting values.

2. Material and Method

2.1. Fractional derivative/integral operators and PI ^{λ} D ^{μ} controller

The first thoughts on the fractional derivative and integral go back to Leibniz and L'Hospital. Although there are many suggestions in the literature regarding the definition of the fractional operator, the definitions of Grünwald–Letnikov, Riemann–Liouville and Caputo are frequently used (Valério & Costa, 2011). The fractional derivative and integral are expressed as follows.

$${}_aD_t^\alpha = \begin{cases} \frac{d^\alpha}{dt^\alpha} & R(\alpha) > 0 \\ 1 & R(\alpha) = 0 \\ \int_a^t (d\tau)^{-\alpha} & R(\alpha) < 0 \end{cases} \tag{1}$$

In the notation in Equation 1, the expression ${}_aD_t^\alpha$ is the fractional operator. α the fractional degree, a and t are limits of the operation. The definition of Grünwald-Letnikov is as follows;

$${}_aD_t^\alpha = \lim_{h \rightarrow 0} \frac{1}{h^\alpha} \sum_{i=0}^{\lfloor \frac{t-a}{h} \rfloor} (-1)^i \binom{n}{i} g(t - ih), \quad n - 1 < \alpha < n \tag{2}$$

In Equation 2, $\lfloor \frac{t-a}{h} \rfloor$ is an integer, and a and t represent its limit. $\binom{n}{i}$ are binomial coefficients and are expressed as follows;

$$\binom{n}{i} = \frac{\Gamma(n + 1)}{\Gamma(i + 1)\Gamma(n - i + 1)} \tag{3}$$

Gamma function in Equation 3 is defined as;

$$\Gamma(n) = \begin{cases} \int_0^\infty t^{n-1} e^{-t} dt & n \in R \\ (n - 1)! & n \in N \end{cases} \tag{4}$$

Riemann–Liouville definition;

$${}_aD_t^\alpha = D^n J^{n-\alpha} f(t) = \frac{1}{\Gamma(n - \alpha)} \left(\frac{d}{dt}\right)^n \int_a^t \frac{f(\tau)}{(t - \tau)^{\alpha-n+1}} d\tau, \quad n - 1 < \alpha < n \tag{5}$$

In Equation 5, n is an integer, α is a real number, a and t are the limits of integration and J is the integral operator.

Another widely used definition is defined by Caputo;

$${}_aD_t^\alpha = \frac{1}{\Gamma(n - \alpha)} \int_a^t \frac{f^n(\tau)}{(t - \tau)^{\alpha-n+1}} d\tau, \quad n - 1 < \alpha < n \tag{6}$$

In Equation 6, n is an integer, a and t are the limits of integration and α is a real number.

The traditional integer PID controller is frequently used in industrial process applications because it provides the desired performance such as easy design, low overshoot, and small settling time (Astrom, 1995). It can be designed in P, PI, or PID forms depending on the type of application. In the form of a general closed-loop PID controller, the error signal is multiplied by the proportional gain (K_p), the error is integrated and multiplied by the integral gain (K_i), the derivative of the error is multiplied by the derivative gain (K_d), and the control signal is obtained by adding these three product values. The K_p , K_i , and K_d gains are the basic characteristics of the PID controller

and the performance of the PID controller depends on these three coefficients. The representations of the integer conventional PID and the $PI^\lambda D^\mu$ controller in Laplace space, respectively, are shown in Equation 7 and Equation 8 below.

$$C_{PID}(S) = K_p + \frac{K_i}{S} + K_d S \tag{7}$$

$$C_{PI^\lambda D^\mu}(S) = K_p + \frac{K_i}{S^\lambda} + K_d S^\mu \tag{8}$$

The degrees of derivative and integral operators in a conventional PID controller are real and integer values. In fractional order PID controller design, derivative and integral operators are expressed using expressions from Equation 1-Equation 6, thus conventional PID controller is expressed as $PI^\lambda D^\mu$. In this notation, λ and μ denote the degrees of the integral and derivative operators, respectively. $PI^\lambda D^\mu$ controllers are less sensitive to parameter changes of the controller and the controlled system than traditional PID controllers (Chao et al., 2010). This is the superiority of $PI^\lambda D^\mu$ controllers. Although they perform better than PID controllers, the fractional derivative and fractional integral operations given in Equation 1-Equation 6 have additional and not easy mathematical operations. To avoid these mathematical difficulties, researchers have proposed some integer approximations (Carlson and Halijak 1964; Charef et al., 1992; Matsuda and Fujii, 1993; Oustaloup et al., 2000; Podlubny et al., 2002). In this study, Matsuda's 6. degree approximate model was used.

2.2. Inverted pendulum system

A classical Inverted pendulum system basically has two components. These; are a pendulum and a carrier car. The pendulum carrier is attached to a freely rotatable hinge on the upper center of the car. The state of motion of the pendulum and the carriage depends on the force applied to the carriage. In the inverted pendulum problem, the aim is to bring the pendulum to a certain reference point by keeping it in a vertical position with the force applied to the carrier car. In this respect, this problem is a single-input-multiple-output (SIMO) control problem. The free-body diagram for the inverted pendulum system is given in Figure 1 below. Here, the inverted pendulum system consists of a wheeled vehicle (cart) that can move in the x -axis direction on the ground and a rod (pendulum) that can move freely in the y -section at the midpoint of this vehicle. The pendulum has two parameters denoted by l and m . l is the length of the pendulum's center of mass of the pendulum, and m is the mass of the pendulum. The wheeled vehicle is expressed with the mass M . The angle that the pendulum makes with the y -axis at the center point of the cart is represented by the variable θ , while the amount of displacement of the cart in the x -axis relative to a fixed reference point is expressed by the variable x . The coefficient of friction between the vehicle and the ground is b .

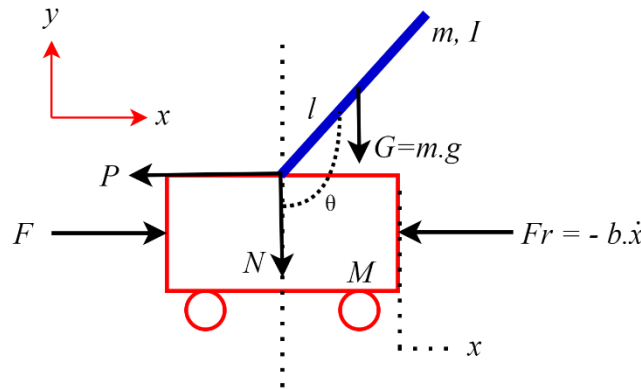


Figure 1. Free body diagram of an inverted pendulum system on a cart.

The symbols used in Figure 1 and the equations below and the values used in the simulation studies are given in Table 2 below.

Table 2. Symbols, descriptions, values, and units used in the study

Symbol	Explanation	Value	Unit
g	Gravitational acceleration	9.8	m/s^2
L	Length of pendulum	0.61	m
l	The distance from the center of mass of the pendulum to the car	0.305	m

M	Mass of the cart	0.455	kg
m	Mass of the pendulum	0.21	kg
G	Weight of the pendulum	2.058	N
F	Force applied to the cart		N
F_r	Frictional force	-	N
b	Coefficient of friction	-	$N \times s/m$
N	Weight component on the x -axis		N
P	Weight component on the Y -axis		N
I	Moment of inertia of the pendulum		$kg \times m^2$
$\ddot{\theta}$	Angular acceleration of the pendulum		rad/s^2
$\dot{\theta}$	Angular velocity of the pendulum		rad/s
θ	Angular position of the pendulum		rad
\ddot{x}	Cart acceleration		m/s^2
\dot{x}	Speed of the cart		m/s
x	Position of the cart		m

In this section, the nonlinear model of the inverted pendulum is found using Newton's laws and linearized around the defined operating point (Michigan, 2022). When Newton's second rule is applied to motion in the x direction;

$$\ddot{x} = \frac{1}{M} \sum_c F_x = \frac{1}{M} (F - N - b\dot{x}) \quad (9)$$

$$\ddot{\theta} = \frac{1}{I} \sum_p \tau = \frac{1}{I} (-Pl \sin \theta - Nl \cos \theta) \quad (10)$$

The dynamic equations of the pendulum in the x and y directions are as follows.

$$N = \sum_p F_x = m\ddot{x}_s \quad (11)$$

$$P = mg + \sum_p F_y = mg + m\ddot{y}_s \quad (12)$$

The x and y position coordinates of the pendulum can be represented by equations as follows.

$$x_p = x + l \sin \theta \quad (13)$$

$$\ddot{x}_p = \ddot{x} - l\dot{\theta}^2 \sin \theta + l\ddot{\theta} \cos \theta \quad (14)$$

$$y_p = -l \cos \theta \quad (15)$$

$$\dot{y}_p = l\ddot{\theta} \sin \theta + l\dot{\theta}^2 \cos \theta \quad (16)$$

The following equations were obtained by using the equivalents in Equation 14 and Equation 16 instead of $\ddot{x}_{pendulum}$ and $\ddot{y}_{pendulum}$ values in Equations 11 and 12.

$$N = m\ddot{x} - ml\dot{\theta}^2 \sin \theta + ml\ddot{\theta} \cos \theta \quad (17)$$

$$P = mg + m(l\ddot{\theta} \sin \theta + l\dot{\theta}^2 \cos \theta) \quad (18)$$

The following equations were obtained by using the equivalents in Equation 17 and Equation 18 instead of N and P values in Equation 9 and Equation 10.

$$M\ddot{x} + m\ddot{x} - ml\dot{\theta}^2 \sin \theta + ml\ddot{\theta} \cos \theta + b\dot{x} = F \quad (19)$$

$$P \sin \theta + N \cos \theta - mg \sin \theta = ml\ddot{\theta} + m\ddot{x} \cos \theta \quad (20)$$

$$-P \sin \theta - N \cos \theta = I\ddot{\theta} \quad (21)$$

$$I\ddot{\theta} + ml^2\ddot{\theta} + mgl \sin \theta = -ml\ddot{x} \cos \theta \quad (22)$$

In order to get rid of the nonlinearity caused by the sin and cos functions in the above equations, the following approximations are made, assuming that the pendulum changes in a small range of ϕ in the equilibrium state.

$$\cos \theta = \cos(\pi + \phi) \approx -1 \quad (23)$$

$$\sin \theta = \sin(\pi + \phi) \approx -\phi \quad (24)$$

$$\dot{\theta}^2 = \dot{\phi}^2 \approx 0 \quad (25)$$

Thus, the following equations are obtained. (Also, u is used instead of F).

$$(M + m)\ddot{x} + b\dot{x} - ml\ddot{\phi} = u \quad (26)$$

$$(I + ml^2)\ddot{\phi} - mgl\phi = ml\ddot{x} \quad (27)$$

$$(M + m)X(s)s^2 + bX(s)s - ml\Phi(s)s^2 = U(s) \quad (28)$$

Taking the Laplace transform at zero initial conditions;

$$(I + ml^2)\Phi(s)s^2 - mgl\Phi(s) = mlX(s)s^2 \quad (29)$$

The transfer functions of the cart and pendulum obtained using Equation 28 and Equation 29 are obtained as shown below.

$$TF_c(s) = \frac{X(s)}{U(s)} = \frac{\frac{(I + ml^2)s^2 - mgl}{q}}{s^4 + \frac{b(I + ml^2)}{q}s^3 - \frac{(M + m)mgl}{q}s^2 - \frac{bmgl}{q}s} \quad \left[\frac{m}{N} \right] \quad (30)$$

$$TF_p(s) = \frac{\Phi(s)}{U(s)} = \frac{\frac{ml}{q}s}{s^3 + \frac{b(I + ml^2)}{q}s^2 - \frac{(M + m)mgl}{q}s - \frac{bmgl}{q}} \quad \left[\frac{rad}{N} \right] \quad (31)$$

Here q ;

$$q = (M + m)(I + ml^2) - (ml)^2 \quad (32)$$

To do simulation work, an inverted pendulum model with a cart can be constructed using Equations 30 and Equations 31. The mathematical expressions created in the literature for the inverted pendulum system are given in the section so far. These statements are essential for analytics-based controller designs and analysis. These expressions were used during the modeling of the inverted pendulum system in Simulink and the realization of simulation studies.

2.3. Design of PI^λD^μ controller based on reference model and optimization

In the study, the optimization-based model reference-based design of the PI^λD^μ controller was carried out in the Simulink environment. The block diagram used is shown in Figure 2.

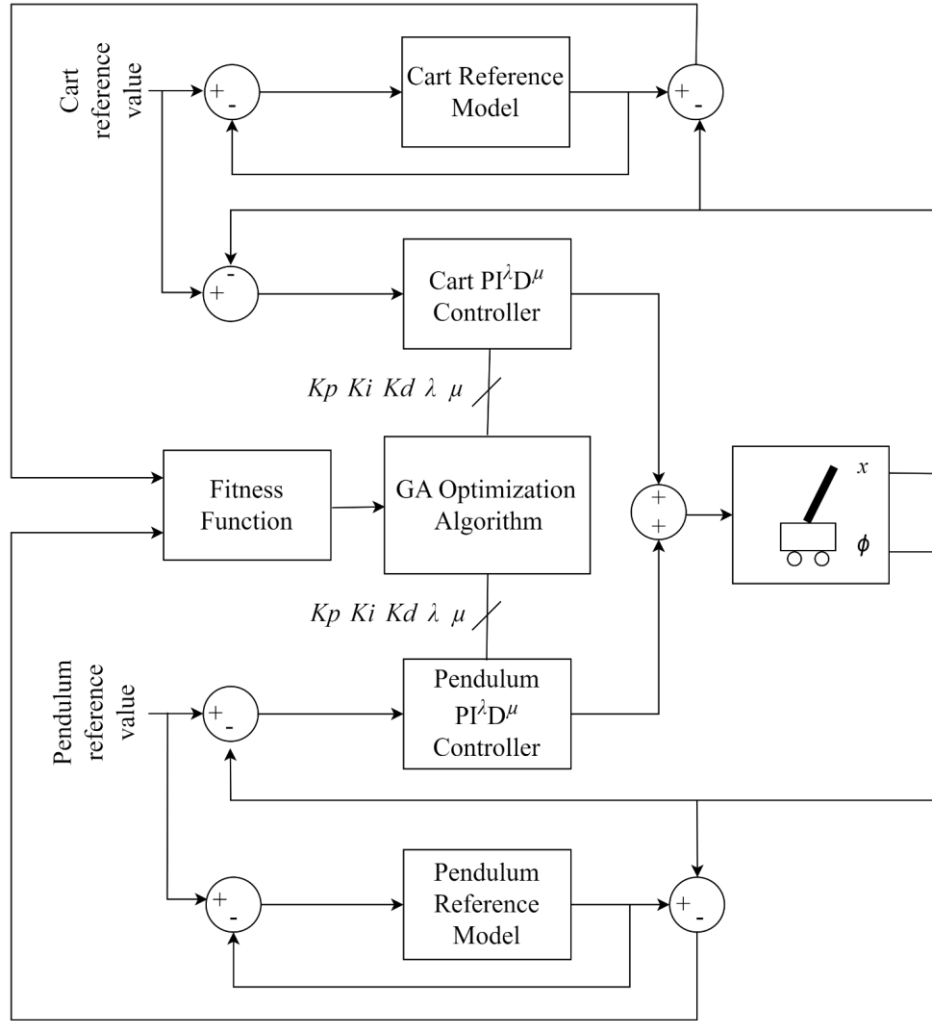


Figure 2. Block diagram representation of the study.

In the block representation in Figure 2, the angular position control of the bar and the vehicle position control were performed with two separate PI^λD^μ controllers. In addition, two predetermined reference models are used for the desired output response of the vehicle position and for the output response of the bar position. The objective function is formed by taking the instantaneous position of the vehicle and the instantaneous position of the bar and the differences between these two reference model outputs. The optimization algorithm tries to reach the objective function to zero value by changing the K_p , K_i , K_d , λ , and μ parameters of the PI^λD^μ controllers by looking at the change of the objective function in each cycle. When the objective function reaches the closest possible value to zero, the vehicle position and the position of the bar converge to the reference model response. Thus, the most suitable K_p , K_i , K_d , λ , and μ parameters for PI^λD^μ controllers are reached. The genetic algorithm was used as the optimization algorithm in the study.

In control systems based on the reference model, it is important to determine the response of an ideal system. Bode's ideal transfer function was used to create the reference models. Bode in 1945, defined the open-loop transfer function of a feedback control system expressed as in Equation 33.

$$L(s) = \left(\frac{\omega_c}{s}\right)^\gamma, \quad \gamma \in R \tag{33}$$

In Equation 33, ω_c is the gain crossover frequency and hence $|L(j\omega_c)| = 1$. The parameter γ is the slope of the amplitude curve and can be expressed as a fractional or integer on a logarithmic scale. The transfer function $L(s)$ is a fractional derivative for $\gamma < 0$ and a fractional integrator for $\gamma > 0$. The closed-loop transfer function with negative unit feedback for Bode's fractional ideal transfer function shown in Equation 34 is given in Figure 3 (Barbosa et al., Doğruer et al.).

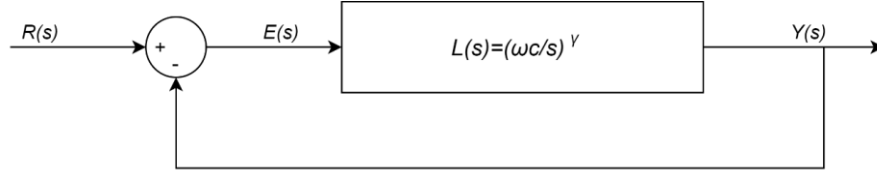


Figure 3. Bode's ideal fractional degree transfer function.

$$T(s) = \frac{L(s)}{1 + L(s)} = \frac{1}{(s/\omega_c)^\gamma + 1}, \quad \gamma \in R^+ \quad (34)$$

In Equation 33, frequency and time domain characteristics can be obtained for different values of ω_c and γ . The following formulas can be used for the unit step characteristics of $T(s)$ (Barbosa et al, 2004).

Overshoot ratio M_p ;

$$M_p = \frac{y_{max} - y(\infty)}{y(\infty)} \quad M_p \approx 0.8(\gamma - 1)(\gamma - 0.75) \quad 1 < \gamma < 2 \quad (35)$$

Peak time T_p (1%);

$$T_p \approx \frac{1.106(\gamma - 0.255)^2}{(\gamma - 0.921)\omega_c} \quad 1 < \gamma < 2 \quad (36)$$

Rising time T_r (1%);

$$T_r \approx \frac{0.131(\gamma + 1.157)^2}{(\gamma - 0.724)\omega_c} \quad 1 < \gamma < 2 \quad (37)$$

Time constant T_c (2%);

$$T_r \approx \frac{0.2(\gamma - 1)^2 + 1}{\omega_c} \quad 1 < \gamma < 2 \quad (38)$$

Settling time T_s (2% and 5%);

$$T_s(2\%) \approx \frac{4}{\cos(\pi - \frac{\pi}{\gamma})\omega_c} = \frac{4}{\zeta\omega_c} \quad 1.39 < \gamma < 2 \quad (39)$$

$$T_s(5\%) \approx \frac{3}{\cos(\pi - \frac{\pi}{\gamma})\omega_c} = \frac{3}{\zeta\omega_c} \quad 1.44 < \gamma < 2 \quad (40)$$

In Equation 39 and 40, $\zeta = \cos(\pi - \pi/\gamma)$ is the damping ratio.

In the study, Bode's ideal transfer function was used as reference model for both the cart and the pendulum. It is aimed that the cart and the pendulum move according to the time domain response appropriate to this model.

3. Simulation Studies

In this section, the determination of the K_p , K_i , K_d , λ and μ parameters of the PI^2D^μ controllers that will control the cart and the pendulum and the results obtained are presented. In the study, for the purpose of comparison, a traditional, in other words, fixed coefficient PID controller was also studied and the results obtained were presented. GA optimization is used for PI^2D^μ and PID controller parameters. The reason why GA optimization is preferred is that it is preferred in many studies. Reference model blocks were created for the cart and pendulum using Bode's ideal transfer function with ω_c ve γ parameter values. After the reference models were created, the GA

optimization process was started. In the optimization process, $PI^{\lambda}D^{\mu}$ and PID controller parameters' lower and upper limit values were taken as given in Table 3.

Table 3. Using lower and upper limit values in optimization

Limit values	Cart					Pendulum		
	K_p	K_i	K_d	λ	μ	K_p	K_d	μ
Lower limit values	-5	-5	-5	0.01	0.01	-5	-5	0.01
Upper limit values	5	5	5	1	1	5	5	1

In the optimization, the population number is set to 30 and the stopping criterion is set to 200 iterations. Equation 41 was used as the fitness function. ITAE was used as a performance criterion.

$$J_{min} = \alpha * ITAE_{cart} + \beta * ITAE_{pendulum} \tag{41}$$

$$ITAE = \int_0^{\infty} t|e(t)|dt \tag{42}$$

In equation 42, t is time, and $e(t)$ is the difference between the output of the cart pendulum and the reference model. α is the ITAE weight for the cart position and β is the ITAE weight for the pendulum position. In the study, optimization studies were carried out for different α and β weighting factors and for gain crossover frequency ω_c and γ parameters in the reference model in Equation 33. In order to provide real environmental conditions, [+10,-10] N control signal saturation block is placed at the input of the pendulum system modeled in the simulation environment. In addition, the working area of the card is determined as [+10,-10] m. When a 10 N input is applied to the cart, the cart travels 7.2 m. Based on this, a reference model was created for the cart by taking $\omega_c = 0.7$ and $\gamma = 1.01$. Thus, sufficient rise time, settling time, and overshoot ratio values were obtained for cart position control. Compared to the cart, the pendulum's range of motion is much shorter. For the pendulum, it is aimed to cover an angle change of 90 in approximately 1 second. For this reason, $\omega_c = 7.07$ and $\gamma = 1.01$ were chosen for the pendulum. In Figure 4 and Figure 5, the reference model's time responses obtained for values of ω_c and γ parameters are shown.

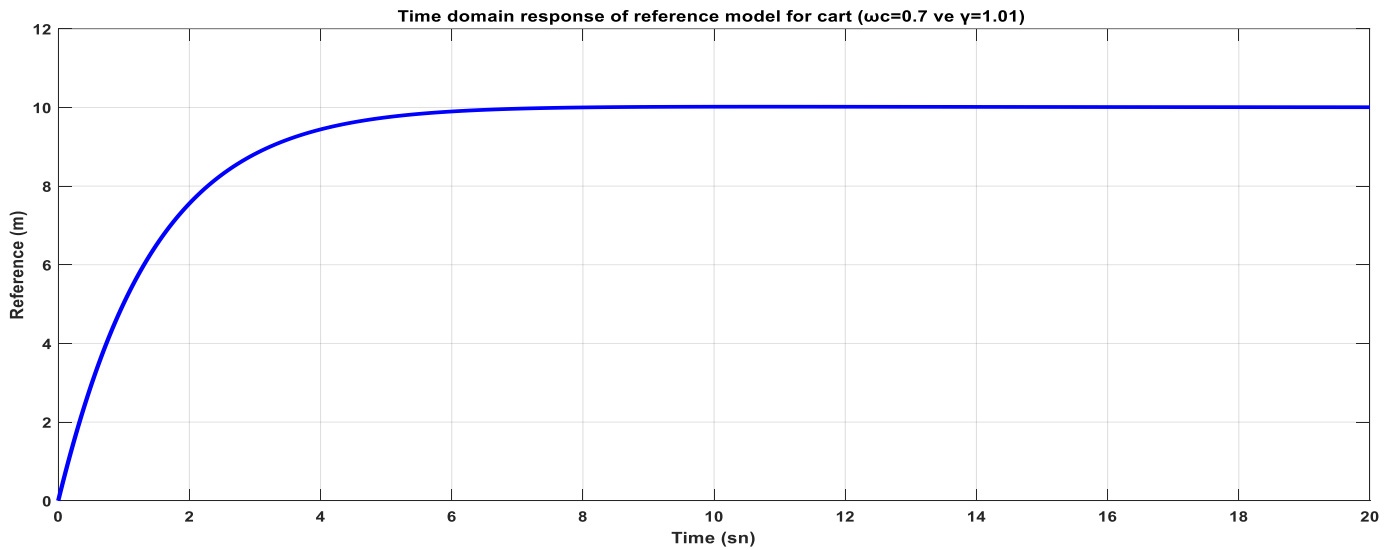


Figure 4. Time responses of the cart reference model for $\omega_c = 0.7$ and $\gamma = 1.01$ values.

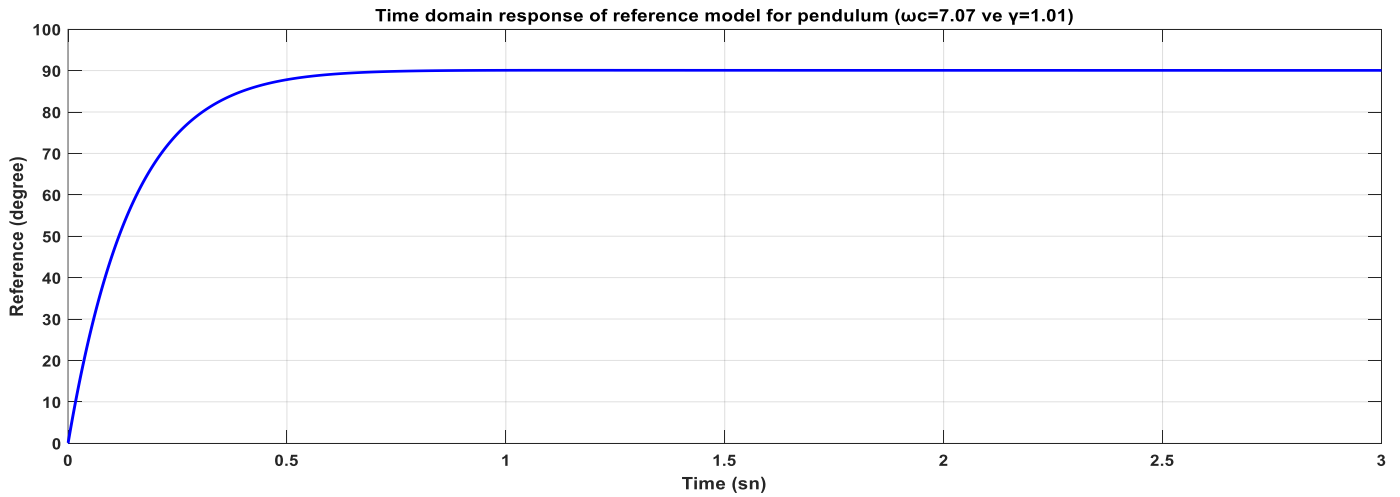
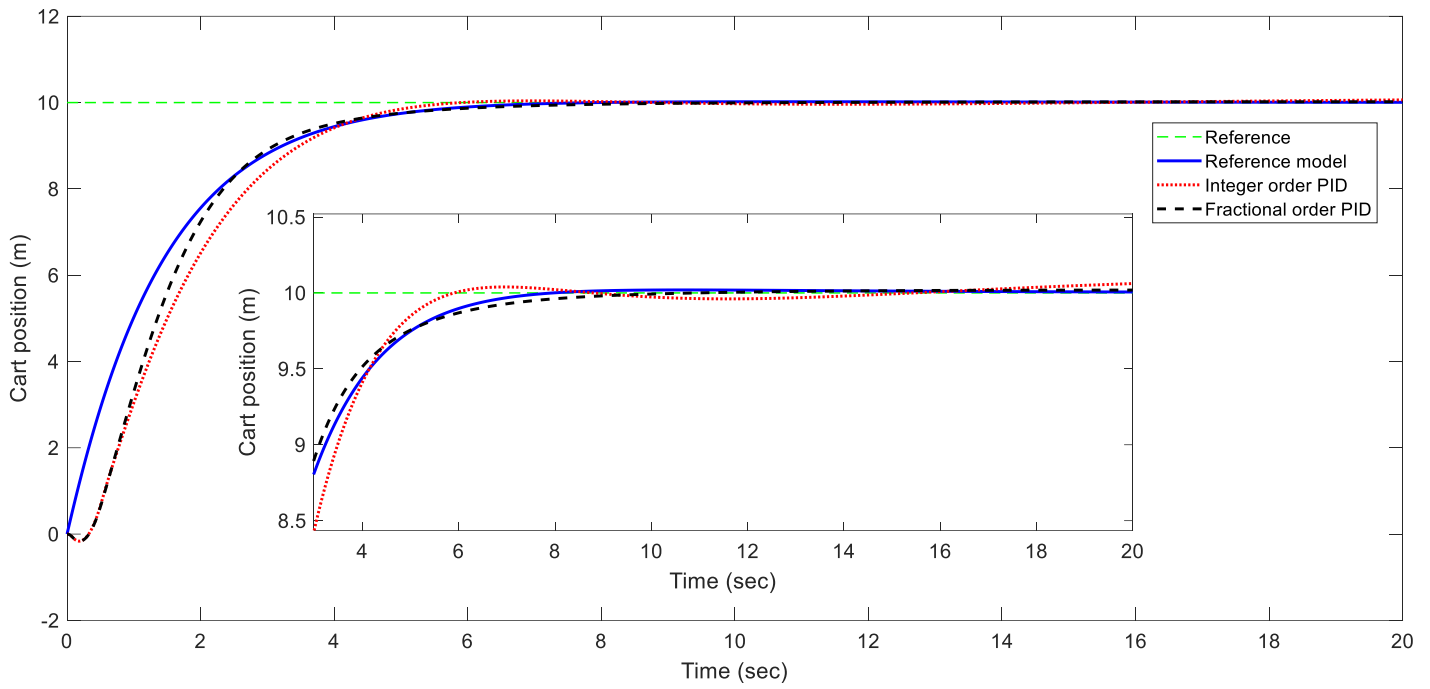


Figure 5. Time responses of the pendulum reference model for different $\omega_c=7.07$ and $\gamma=1.01$ values.

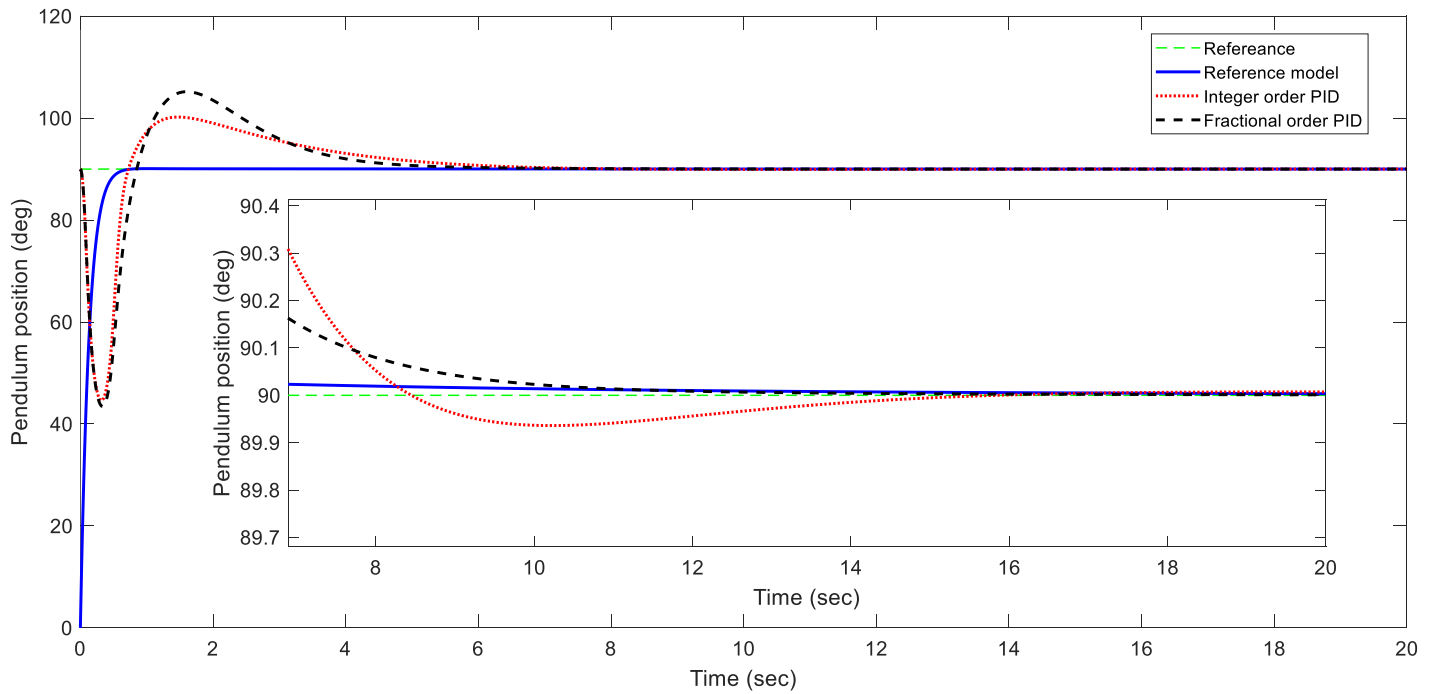
The simulation studies were repeated for different α and β parameters. Thus, the effects of α and β parameters in the fitness function given in Equation 41 on the controller design performance were investigated. As a result of repeated studies, it was seen that the fitness function was minimized at a good rate for the weight values of $\alpha=0.9$ and $\beta=0.1$, and the cart and pendulum references could be captured well. Controller parameters obtained as a result of the GA optimization are given in Table 4. Obtained control results using the controller parameters in Table 4 for constant reference are also presented in Figure 6.

Table 4. Obtained controller parameters using the optimization

Controllers	Obtained parameters							
	Cart					Pendulum		
	K_p	K_i	K_d	λ	μ	K_p	K_d	μ
PID	-0.532	-0.0078	-2.771	-	-	0.720	0.111	-
PI ^{λ} D ^{μ}	-1.364	-0.049	-3.575	0.342	0.951	0.571	0.130	0.916



(a)



(b)

Figure 6. Cart and pendulum positions for constant reference value according to optimization results. (a) Cart position, (b) Pendulum position.

The position control graph of the cart is given in Figure 6.a, and the position control graph of the pendulum is given in Figure 6.b. As a result of the optimization, as seen in Figure 6.a, it was possible to approach the reference model more with the PI^2D^μ controller. In Figure 6.b, the PI^2D^μ controller has a larger overshoot than the other integer-order PID controller, but the reference model can be approached in a shorter time. In Table 5, ITAE values of the error between the position outputs and the reference model of the PI^2D^μ and integer-order PID controllers are presented for comparison purposes. ITAE values show that the output obtained from the PI^2D^μ controller is getting closer to the reference model.

Table 5. ITAE performance indices of PID and $PI^{\lambda}D^{\mu}$ controllers for constant references

Controllers	ITAE performance values	
	Cart	Pendulum
PID	27.9117	77.4239
$PI^{\lambda}D^{\mu}$	23.4737	76.4408

The study was repeated for different reference values. Cart and pendulum time response graphs according to different cart reference values are presented in Figure 7, and ITAE values are shown in Table 6 for comparison of the results obtained.

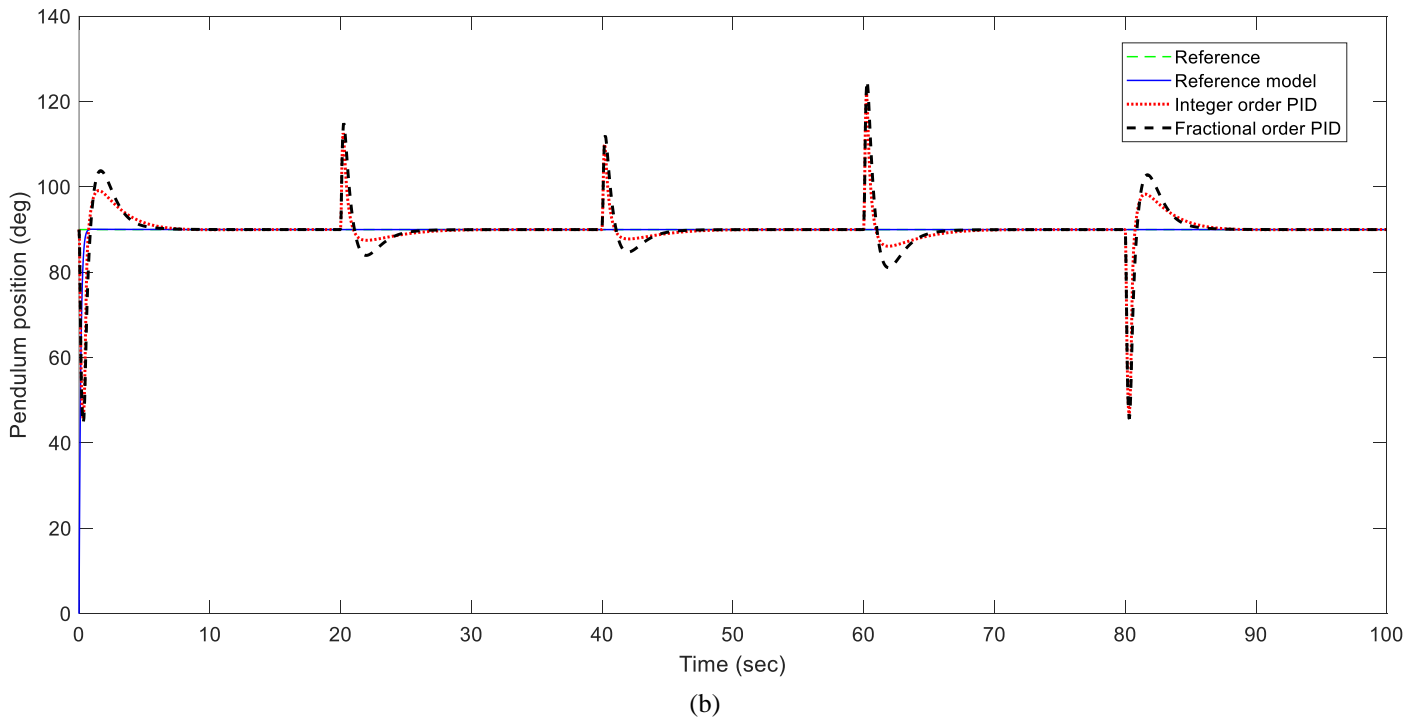
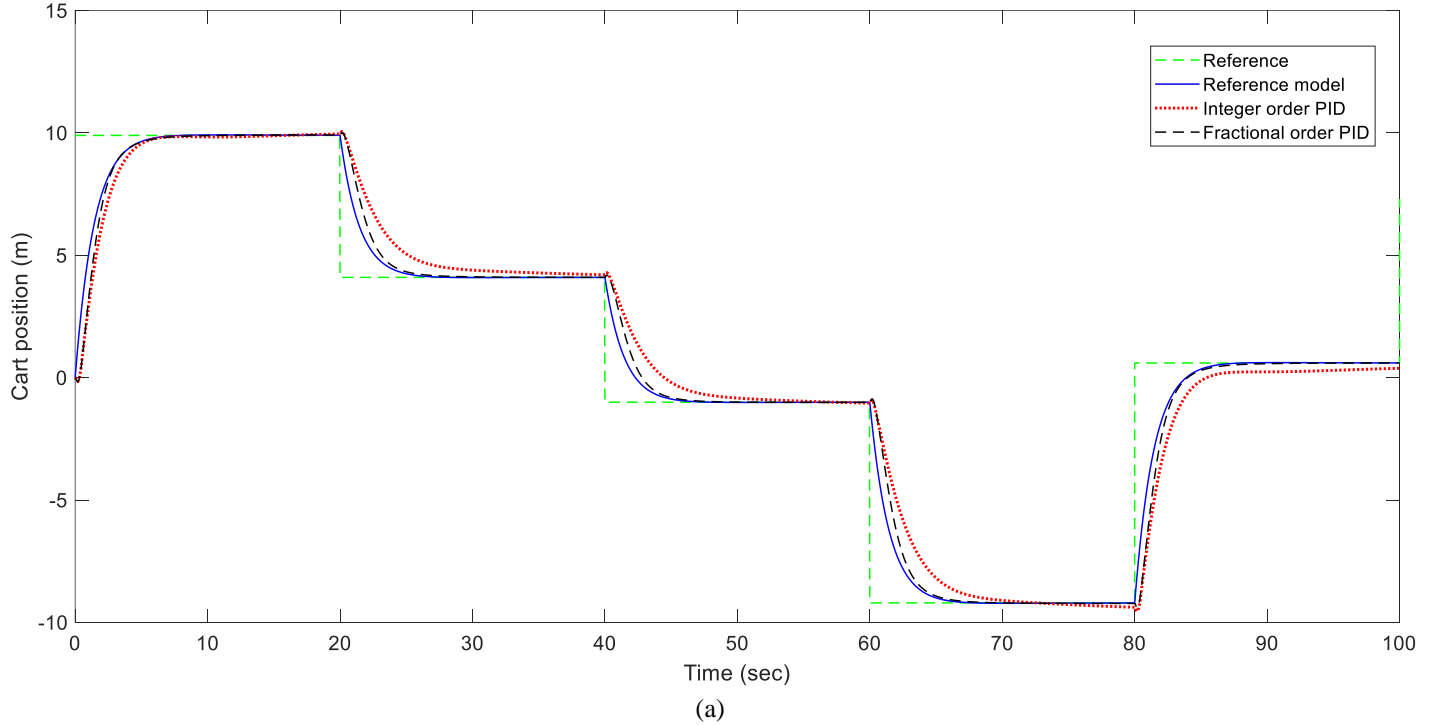


Figure 7. Cart and pendulum positions for different references according to optimization results. (a) Cart position, (b) Pendulum position.

Table 6. ITAE performance indices of PID and $PI^{\lambda}D^{\mu}$ controllers for different references

Controllers	ITAE performance indices	
	Cart	Pendulum
PID	4707.8	6032.0
$PI^{\lambda}D^{\mu}$	3097.2	7793.7

Figure 7.a shows the position change of the cart. Obviously, with the $PI^{\lambda}D^{\mu}$ controller, the reference value could be captured much better with short rising and settling times. It is seen that the rising time and settling time are longer in the output response obtained for the integer-order PID controller. For this reason, the ITAE value given in Table 6 is lower in the $PI^{\lambda}D^{\mu}$ controller. In the pendulum position change graph in Figure 7.b, it is seen that there is a little overshoot in both controllers, but the overshoot value is slightly larger in the $PI^{\lambda}D^{\mu}$ controller. Accordingly, as seen in Table 6, the ITAE value in the pendulum was also slightly higher.

4. Results and Discuss

This study, it is aimed to find the parameters of the $PI^{\lambda}D^{\mu}$ controller with the GA optimization method according to the time domain responses of reference models. The same study was also carried out for the PID controller for comparison purposes. The study was carried out as a simulation study on an inverted pendulum system with a single-input multiple-output (SIMO) structure. In the inverted pendulum system, two separate $PI^{\lambda}D^{\mu}$ and PID controllers and two separate reference models are used for the cart and the pendulum. With the GA optimization, the output response of the inverted pendulum system can be approximated to the reference model by adjusting the K_p , K_i , K_d , λ , and μ parameters of these two controllers. Bode's ideal transfer function of fractional order is used as the reference model. Reference models were obtained for different values of ω_c and γ parameters in Bode's ideal transfer function.

In the GA optimization, a fitness function based on the α -weighted ITAE value for the cart and the β -weighted ITAE value for the pendulum is used. Sequential simulation studies were carried out for different α and β parameters in the fitness function and for different ω_c and γ parameter values in the reference models. Thus, the effects of these parameters on the controller design performance were investigated. According to the results obtained by the simulation studies, it has been observed that the α and β parameters in the fitness function seriously affect the controller performance in the position control of the cart and the angle control of the pendulum in the inverted pendulum system. By increasing the α factor, the cart position output approaches the reference model created for the position. Similarly, by increasing the β weight factors, the angle output of the pendulum approaches its reference model. As a result of repeated studies, the best results were obtained for the weighting factors of $\alpha=0.9$ and $\beta=0.1$ in the optimization function. The selection of α and β weight factors according to the desired performance expectations from the system is important in terms of design. As a continuation of the study, carrying out the proposed method on a real inverted pendulum system will be useful for the confirmation of the findings.

References

- Astrom KJ. (1995). PID controllers: theory, design and tuning. Instrt Soc Am.
- Azarmi R., Tavakoli-Kakhki M., Sedigh A. K. & Fatehi A. (2015). Analytical design of fractional order PID controllers based on the fractional set-point weighted structure: Case study in twin rotor helicopter, *Mechatronics* Volume 31, 222-233.
- Barbosa R. S., Machado J. A. T. & Ferreira I. M., (2004). Tuning Of Pid Controllers Based On Bode's Ideal Transfer Function, *Nonlinear Dynamics* 38: 305–321.
- Bouafoura M. K. & Braiek N. B. (2010). $PI^{\lambda}D^{\mu}$ controller design for integer and fractional plants using piecewise orthogonal functions. *Communications in Nonlinear Science and Numerical Simulation*, 15 (5), 1267-1278.
- Carlson G. & Halijak C. (1964). Approximation of fractional capacitors (1/s)(1/n) by a regular Newton process, *IEEE Transactions on Circuit Theory*, 11:2, 210-213.
- Castillo F.J., Feliu V., Sánchez L., Rivas R. & Jaramillo V.H. (2010). Robust PD^{α} Time-Domain Tuning Rules for Controlling DC-Motors. The 4th IFAC Workshop Fractional Differentiation and its Applications, Badajoz, Spain.
- Castillo F.J., Feliu V., Sánchez L., Rivas R. & L.Sánchezc. (2010). Design of a class of fractional controllers from frequency specifications with guaranteed time domain behavior. *Computers & Mathematics with Applications*, 59(5), 1656-1666.
- Charef A., Sun H., Tsao Y. & Onaral B. (1992). Fractal system as represented by singularity function, *IEEE Transactions on Automatic Control*, 37:9, 1465-1470.

- Chao H., Luo Y., Di L. & Chen Y.Q. (2010). Roll-channel fractional order controller design for a small fixed-wing unmanned aerial vehicle. *Control Eng Prac* 18(7), 761–72.
- Deniz F. N., Yüce A. & Tan N. (2019). Tuning of PI-PD Controller Based on Standard Forms for Fractional Order, 8 (1), 5-21.
- Deniz F. N., Yüce A., Tan N. & Atherton D. P. (2017). Tuning of Fractional Order PID Controllers Based on Integral Performance Criteria Using Fourier Series Method, *IFAC PapersOnLine* 50-1, 8561–8566.
- Doğruer T., Yüce A. & Tan N. (2017). PID Controller Design Using Optimization Method for Fractional Order Control Systems with Time Delay, *Gaziosmanpaşa Journal of Scientific Research*, 6, Special Issue, (ISMSIT2017), 30-39.
- Doğruer T., Yüce A. & Tan N. (2017). PID Controller Design Based on Reference Model in Fractional Order Control Systems, *Bilge International Journal of Science and Technology Research*, 1 (1), 52-58.
- Doğruer T. & Tan N., (2020). Real Time Control of Twin Rotor MIMO System With PID and Fractional Order PID Controller, *Mugla Journal Of Science And Technology* 6, 1-9.
- El-Khazali R. (2013). Fractional-order $PI\lambda D\mu$ controller design, *Computers & Mathematics with Applications* Volume 66, Issue 5, 639-646.
- Hamamci S. E & Koksal M. (2010). Calculation of all stabilizing fractional-order PD controllers for integrating time delay systems. *Computers & Mathematics with Applications*, 59 (5), 1621-1629.
- Keyser R. D., Muresan C. I. & Ionescu C. M. (2016). A novel auto-tuning method for fractional order PI/PD controllers, *ISA Transactions* Volume 62, 268-275.
- Keyser R. D., Muresan C. I. & Ionescu C. M. (2018). “Autotuning of a Robust Fractional Order PID Controller”, *IFAC PapersOnLine* 51-25, 466–471.
- Luo Y. & Chen Y.Q. (2009). Fractional-order [Proportional Derivative] Controller for Robust Motion Control: Tuning Procedure and Validation, 2009 American Control Conference, St. Louis, Missouri, USA.
- Matsuda K. & Fujii H. (1993). H (infinity) optimized wave-absorbing control Analytical and experimental results, *Journal of Guidance, Control, and Dynamics*, 16:6, 1146-1153.
- Michigan. (2022). Author. Retrieved from <https://ctms.engin.umich.edu/CTMS/index.php?example=InvertedPendulum§ion=SystemModeling>
- Muresan C. I., Dulf E. H. & Both R. (2016). Vector-based tuning and experimental validation of fractional-order PI/PD controllers, *Nonlinear Dyn*, 84, 179–188.
- Muresan C. I. & Keyser R. D., (2022). Revisiting Ziegler–Nichols. A fractional order approach, *ISA Transactions* Volume 129, Part A, 287-296.
- O’Dwyer A.. (2006). Handbook of PI and PID Controller Tuning Rules, Imperial College Press, <http://dx.doi.org/10.1142/9781860949104>
- Oustaloup A., Levron F., Mathieu B. & Nanot F. M.. (2000). Frequency-band complex noninteger differentiator: characterization and synthesis, *IEEE Transactions on Circuits and Systems I: Fundamental Theory and Applications*, 47:1, 25-39.
- Ozyetkin M. M, Onat C. & Tan N. (2020). PI-PD controller design for time delay systems via the weighted geometrical center method. *Asian Journal of Control*, 22 (5), 1811-1826.
- Podlubny I. (1999). Fractional-Order Systems and $PI\lambda D\mu$ -Controllers, *IEEE Transactions on Automatic Control*, 44(1), 208 - 214.
- Podlubny I., Petráš I., Vinagre B. M., O’leary P. & Dorčák Ľ. (2002). Analogue realizations of fractional-order controllers, *Nonlinear dynamics*, 29,1-4, 281-296.
- Shah P. & Agashe S. (2016). Review of fractional PID controller, *Mechatronics* 38, 29–41,

Shankaran V. P., Azid S. I. & Mehta U., (2022). Fractional-order PI plus D controller for second-order integrating plants: Stabilization and tuning method, *ISA Transactions* Volume 129, Part A, 592-604.

Valério D. & da Costa JS. (2011). Introduction to single-input, single-output fractional control. *IET Control Theory Appl* 5(8), 1033–57.

Yeroglu C. & Tan N.. (2011). Note on fractional-order proportional–integral–differential controller design, Volume 5, Issue 17, 1978 – 1989.